Sodium Glycodeoxycholate and Glycocholate Mixed Aggregates in Gas and Solution Phases

Giulia de Petris,[§] Maria Rosa Festa,[†] Luciano Galantini,*[,†,‡] Edoardo Giglio,[†] Claudia Leggio,[†,‡] Nicolae Viorel Pavel,[†,‡] and Anna Troiani*[,§]

Dipartimento di Chimica, Research Center SOFT-INFM-CNR, and Dipartimento di Chimica e Tecnologie del Farmaco, Sapienza Università di Roma, P. le Aldo Moro 5, 00185 Roma, Italy

Received: February 5, 2009; Revised Manuscript Received: April 1, 2009

This paper deals with electrospray ionization mass spectrometry (ESIMS), small-angle X-ray scattering (SAXS), and dynamic light scattering (DLS) measurements in order to provide information on the existence, aggregation, composition, and structure of the two-component aggregates of sodium glycocholate (NaGC) and sodium glycodeoxycholate (NaGDC) in the gas and solution phases. Five samples, containing 100% NaGC and 100% NaGDC, and NaGDC/NaGC molar ratios of 3 (75D), 1 (50D), and 1/3 (25D), have been analyzed by ESIMS in positive-ion detection mode starting from 10^{-3} and 10^{-2} M total bile salt concentration in aqueous solutions. Generally, dimers or trimers prevail in the 100% NaGC or NaGDC samples, respectively, as observed in the preceding one-component ESIMS measurements and in agreement with the proposed micellar aggregate structures in aqueous solution. Moreover, it is observed that the composition of multimers in the samples 75D, 50D, and 25D deviates from the one expected on the basis of a random association of the monomers, the NaGDC contribution generally prevailing on the NaGC one. It happens also under the same percentage condition (50D sample), in agreement with a greater aggregation ability of NaGDC with respect to NaGC. SAXS and DLS data were recorded on six samples containing a NaGC + NaGDC 40 mM total concentration, one bile salt having 40, 32, 24, 16, 8, and 0 mM concentration and the other the complementary one, keeping constant the NaCl concentration (0.6 M). The NaGDC 40 mM sample presents SAXS curves in agreement with a cylindrical shape of the aggregates as shown in a previous paper. For the bile salt mixtures, the progressive decrease of the sizes and change of the aggregate morphology, toward a globular-like geometry, are observed by increasing the NaGC fraction, thus confirming the hypothesis about the ability of trihydroxy salts to inhibit the growth of dihydroxy salt aggregates. Fits on the basis of cylindrical model can be accomplished for all the SAXS spectra, however, when the extracted cylinder parameters are used to estimate theoretical hydrodynamic radii a reasonable agreement is obtained only for the samples at high fraction of NaGDC (NaGDC $\geq$ 24 mM).

Introduction

Bile salts show surface-active and detergent-like properties and are able to form in aqueous solutions micellar aggregates[1−4] that solubilize and interact with several important biological compounds (for instance, phospholipids, proteins, cholesterol, fatty acids, bilirubin-IXα, etc.) by means of weak forces. In the light of these properties, a lot of studies have been carried out aimed at describing the biological activities of bile salts and their possible technological applications. In particular, the self-assembly properties of natural bile salt have been extensively investigated[5−13] along with those of more complex systems such as bile salt/lecithin mixtures,[14−17] bile salt containing catanionic aggregates[18,19] or solutions of derivatives obtained by chemical modifications of natural bile salts.[10−24]

The knowledge of the structure of natural bile salt micelles is of paramount importance for establishing their biomedical behavior and plenty of literature is available reporting about controversial models.[25,26] Our experimental evidence supported that dimers and their multiples (mainly octamers and hexadecamers) or 7/1 helices formed by trimers suitably represent the trihydroxy or the dihydroxy bile salts one-component micellar aggregate structures in aqueous solutions, respectively.[27−30] The examined trihydroxy or dihydroxy compounds were sodium glycocholate (NaGC) and taurocholate (NaTC) or sodium glycodeoxycholate (NaGDC) and taurodeoxycholate (NaTDC). On the other hand, by utilizing electrospray ionization mass spectrometry (ESIMS)[31−33] to study the formation of NaGC, NaGDC, NaTC, and NaTDC one-component aggregates in the gas phase, it was found that small size aggregates, analogous to those present in aqueous micellar solutions, occur.[34]

Although solutions of single natural bile salts have been mainly investigated, it is important to remark that the study of bile salt mixtures is by far more important from a biological point of view. As a matter of fact, the bile salts exert their activity mainly in systems containing, generally, more than one bile salt, besides many other compounds. As a first step toward the investigation of biological very complex systems, a study of a binary mixture of two bile salts was carried out in this work. In particular, solutions containing both NaGC and NaGDC were analyzed. A preliminary investigation of solutions of bile salt binary mixtures was performed by dynamic light scattering (DLS). The results showed that small amounts of a trihydroxy bile salt (NaGC or NaTC) inhibit the growth of the dihydroxy bile salt (NaGDC or NaTDC) micelles, giving rise to two-component aggregates of size smaller than those of the dihy-

* Corresponding authors. Tel.: (+39)-06-49913687; fax: (+39)-06-490631; e-mail: l.galantini@caspur.it (L.G.). E-mail: anna.troiani@uniroma1.it (A.T.).
[§] Dipartimento di Chimica e Tecnologie del Farmaco.
[†] Dipartimento di Chimica.
[‡] Research Center SOFT-INFM-CNR.

10.1021/jp9010586 CCC: $40.75
Published on Web 04/29/2009

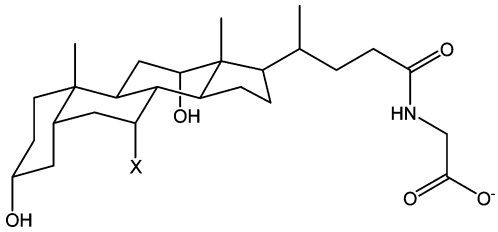

Figure 1. Molecular formula of glycodeoxycholate (X = H) and glycocholate (X = OH) anions.

droxy bile salt alone.[35] The inhibition is greater when bile salts with different polar heads are mixed (NaTC + NaGDC). Conversely, intermediate micellar size, between those of pure NaGDC and NaTDC, are obtained when the mixture of two dihydroxy salts are considered.[36] Electromotive force (EMF) measurements carried out on systems formed by both NaGC and NaGDC confirmed the formation of two-component aggregates, containing both the bile salt anions, the glycocholate aggregation numbers being even and those of glycodeoxycholate being always a multiple of three.[37]

By starting from these conclusions, a detailed study was performed in the present work by combining small-angle X-ray scattering (SAXS), DLS, and ESIMS techniques to get information mainly on the oligomeric structural models of two-component bile salt micellar aggregates, in solution of NaGDC/NaGC mixture. The ESIMS previous results, on one-component micellar aggregates, showed that this technique is suitable to investigate structural features of noncovalent aggregates formed by means of polar (ion−ion, ion-dipole, dipole−dipole, hydrogen bonding, etc.) and apolar (van der Waals and repulsive) interactions.[34] This work constitutes an extension of the applications of this technique in the analysis of the more complicated two-component self-organizing systems.[35] In particular, ESIMS could provide the small NaGDC/NaGC oligomer (for example, dimers, trimers, and tetramers) real compositions which is difficult to foresee with other techniques, owing to the similar structures of the two bile salt anions (Figure 1).

Experimental Section

Materials. NaGDC and NaGC (Sigma, ≥97%) were crystallized in a mixture of water and acetone. Crystals were heated at 60 °C under a pressure of 10^{-2} Torr for 1 day to remove water and acetone before preparing the aqueous electrolyte solutions. NaCl (Merck, Suprapur) was used.

SAXS Measurements. SAXS experiments were performed on the SAXS station at the Dutch-Belgian beamline (DUBBLE), BM26B, at the European Synchrotron Radiation Facility in Grenoble, France.[38] Scattering curves were recorded within the range $0.012 \leq k \leq 0.5$ Å^{-1} ($k = 4\pi \sin\theta/\lambda$). The data recorded were a quarter of the solid angle diffusion and were collected with a gas multiwire two-dimensional detector, 13 × 13 cm^2, with a pixel size of about 250 μm at a sample-to-detector distance of 3 m by using an X-ray wavelength of 1.24 Å (10 keV). The monochromatic incident light from the radiation spectrum of the source was obtained by using a double crystal Si (111) monochromator with sagittal focusing on the second crystal to give an intense monochromatic X-ray beam in the range from 5 to 30 keV. The beam had fixed 0.3 × 0.3 mm^2 output slits and a transmission bandwidth of $\Delta\lambda/\lambda \sim 2 \times 10^{-3}$. Silver behenate was used as a low-angle diffraction standard to check the proper alignment and to calibrate the instrumentation.[39] The samples were filled in 2 mm diameter sealed Lindemann capillaries and kept in thermostated sample holder at 25 °C. SAXS data were subsequently normalized to the intensity of the primary beam for absorption and for detector uniformity and were radially averaged. Experimental scattering curves were converted to absolute intensities expressed in electrons^2/Å^3 (eu = 7.940 56 × 10^{-2} cm^{-1}) by means of an elastomer standard with a known scattering intensity. The observed intensities were corrected for the contribution of the solvent-filled capillary under identical conditions. The scattered intensity $I(k)$ was considered dependent on the form factor alone, since very probably in our samples particle interactions can be neglected. Physically, this means that the scattering centers are not confined to be at "preferred distances" as dictated by intermolecular potentials. Thus

$$I(k) = \int_0^\infty p(r)\frac{\sin(kr)}{kr}\,\mathrm{d}r$$

where $p(r)$ is the electron pair distribution function, which depends on the shape and size of the scattering particles, and vanishes at the maximum electron pair distance within the particles (D_M). Starting from intensities, the indirect Fourier transform method of the ITP program[40] allowed us to calculate the $p(r)$ function, the zero angle intensity, and the electronic radius of gyration (R_g), paramount parameters to verify the aggregate geometry.

For rodlike particles, the scattered intensity can be expressed, in terms of a function $I_c(k)$, which is related only to the cross section. From the innermost part of the $I_c(k)$ curve, it is possible to obtain the radius of gyration of the cross section, R_c, according to the equation

$$I_c(k) = I_c(0)\exp\left(-\frac{k^2 R_c^{\,2}}{2}\right)$$

Moreover, the height can be estimated as

$$h = \pi\frac{I(0)}{I_c(0)}$$

For a homogeneous rod, R_g can be expressed as

$$R_g^{\,2} = \frac{h^2}{12} + \frac{a^2}{2}$$

where a is the cross section radius and is given by $a = \sqrt{2}R_c$. Therefore, an alternative height value (h^*) can be estimated on the basis of the SAXS parameters as

$$h^* = [12(R_g^{\,2} - R_c^{\,2})]^{1/2}$$

DLS Measurements. Brookhaven instrument constituted by a BI-2030AT digital correlator with 136 channels and a BI-200SM goniometer was used. The light source was a Uniphase solid-state laser system model 4601 operating at 532 nm. Dust was eliminated by means of a Brookhaven ultrafiltration unit (BIUU1) for flow-through cells, the volume of the flow cell being about 1.0 cm^3. Nucleopore filters with a pore size of 0.1 μm were used. The samples were placed in the cell for at least 30 min prior the measurement to allow for thermal equilibration. Their temperature was kept constant within 0.5 °C by a circulating water bath. Measurements (laser power 50 mW) were repeated after 24 and 48 h to be sure that data were reproducible.

DLS measurements provided the intensity autocorrelation function $g_2(\tau)$ from which the normalized field autocorrelation function $g_1(\tau)$ is inferred by means of the relation[41,42]

$$g_2(\tau) = 1 + Bg_1^{\,2}(\tau)$$

where B is an instrument factor. According to the cumulant expansion we have

$$\ln g_1(\tau) = -\mathbf{k}^2 D_a \tau + \frac{\mu_2 \tau^2}{2} + ...$$

where **k** is the scattering vector, D_a is the apparent diffusion coefficient, and μ_2 is the so-called second cumulant.

The apparent diffusion coefficients did not depend on the exchanged wave vector in the range 30−150° in our experimental conditions. Therefore, the time-dependent light scattering correlation function was analyzed only at the 90° scattering angle. Scattering decays were analyzed by means of cumulant expansion up to second order, because higher order contributions did not improve the statistics. From the D_a values the hydrodynamic radii R_h were estimated by the Stokes−Einstein equation

$$R_h = \frac{k_B T}{6\pi\eta D_a}$$

where k_B is the Boltzmann constant, T is the absolute temperature and η is the solvent viscosity.

ESIMS Measurements. ESIMS experiments were performed on a ZabSpec oa-TOF multisector mass spectrometer equipped with an electrospray ionization source operating in the positive ion mode (VG Micromass). Samples were directly infused into the electrospray source via a syringe pump at a flow rate of 2 μL/min. Nitrogen was used as nebulizing and drying bath gas at a flow rate of, respectively, 0.2 and 5 L/min. Source temperature was held at about 80 °C to ensure efficient desolvation, and the ESI spray needle was maintained at 4 kV.

Mass spectra were acquired at a low voltage (LNS, 20 V) and high voltage (HNS, 250 V) difference conditions between the nozzle and the skimmer elements. The latter conditions were used to minimize formation of multicharged aggregates. Aqueous solutions 10^{-3} and 10^{-2} M containing a mixture of NaGDC (m/z = 471.3) and NaGC (m/z = 487.3) were analyzed under high-voltage conditions. 10^{-2} M solutions and a flow rate of 20 μL/min were used when acquiring spectra under low-voltage conditions. Results were compared to those obtained from one-component bile salt solutions[34] at the same concentrations.

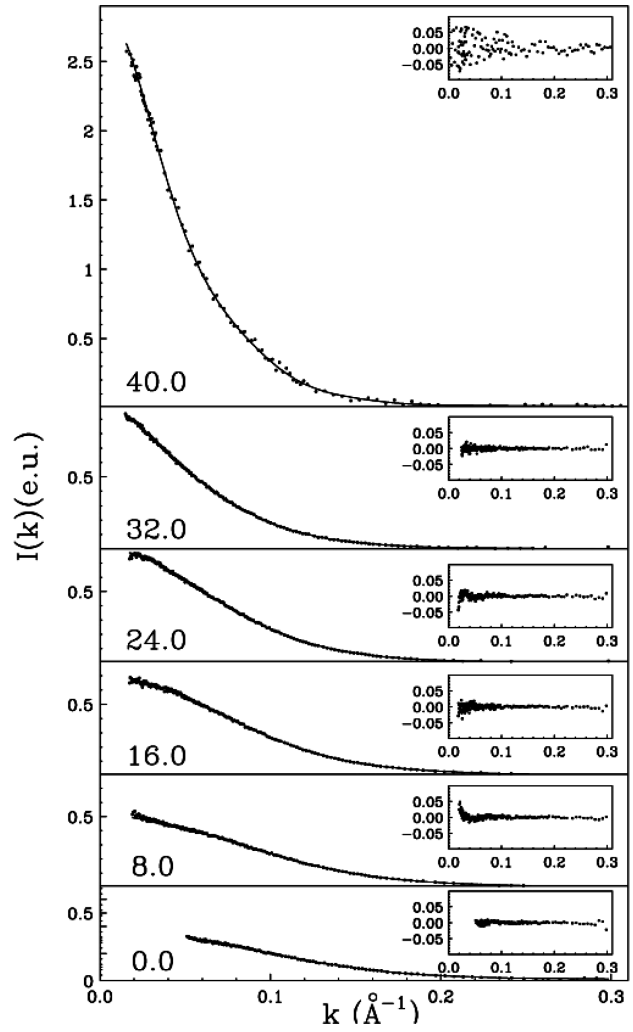

Figure 2. SAXS spectra of NaGC + NaGDC (40 mM) at NaCl 0.6 M. Only the NaGDC concentrations (mM) are reported. The residuals are shown in the insets.

Results and Discussion

SAXS of Two-Component (NaGC and NaGDC) Samples. Six samples with NaGC 0, 8, 16, 24, 32, and 40 mM and with NaGDC 40, 32, 24, 16, 8, and 0 mM, respectively, have been studied at 25 °C in electrolyte aqueous solutions containing NaCl 0.6 M to minimize charge interactions. Their scattering intensities, $I(k)$, and electron pair distance distribution functions, $p(r)$, are reported in Figures 2 and 3. Table 1 collects the most relevant parameters of SAXS spectra recorded at 25 °C and with NaCl concentration 0.6 M, together with the observed apparent hydrodynamic radii. These data do not conflict with those formerly published on NaGDC micellar aggregates using SAXS and DLS techniques.[43−45]

In a previous paper we reported SAXS and DLS results on NaGDC solutions at different concentration and we observed that at 0.6 M NaCl the micellar interactions are negligible for samples up to 40 mM NaGDC concentration. This result supports the data for the sample with the biggest NaGDC concentration (Table 1) and allows us to claim that it has aggregates cylindrical in shape. On the other side, for the pure NaGC sample the SAXS and $p(r)$ curves point out a globular-like shape of the micelles. In particular, the R_g and D_M values are in good agreement with those expected for a model formed by octamers which can be represented by a squared cross section with an edge of about 26 Å, as observed in the NaGC crystal and fiber structures.[46,47] Considering a prism with edges 30 × 30 × 20 Å (assuming a 2 Å hydration thickness) for the hexadecamer, the calculated R_g and D_M are 14 and 40 Å, respectively, in agreement with the corresponding experimental values of 13.5 and 38 Å. A logical gradual change of the micelle morphology is expected along the sample set, in view of the differences in the aggregate geometries of the two limit samples (NaGDC and NaGC pure solutions). This trend is clearly outlined by the progressive variation of the $p(r)$ curves (Figure 3).

Despite this, by imposing a cylindrical shape of the micelles, the particle R_c and heights were inferred for all the samples, and decreasing values were obtained by increasing the NaGC fraction. However, for the samples at NaGDC ≤ 16 mM, we observed that the extraction of these parameters is very difficult, thus indicating that they represent only apparent values, whose decreasing trend reflects a more complex and drastic change of the particle structure. It is important to remark that, as mentioned in the experimental material, all these data were inferred under the assumption of negligible particle interaction. This approximation, which has been already proved for the pure NaGDC sample, can be reliably applied to all the investigated solutions because they have the same NaCl concentration and surfactant total volume fraction (NaGDC and NaGC molecular formulas and volumes,[48,49] about 620 Å^3, being nearly equal). As a matter of fact, in these conditions a relevant increase of the interaction effect, in the mixed and pure NaGC samples,

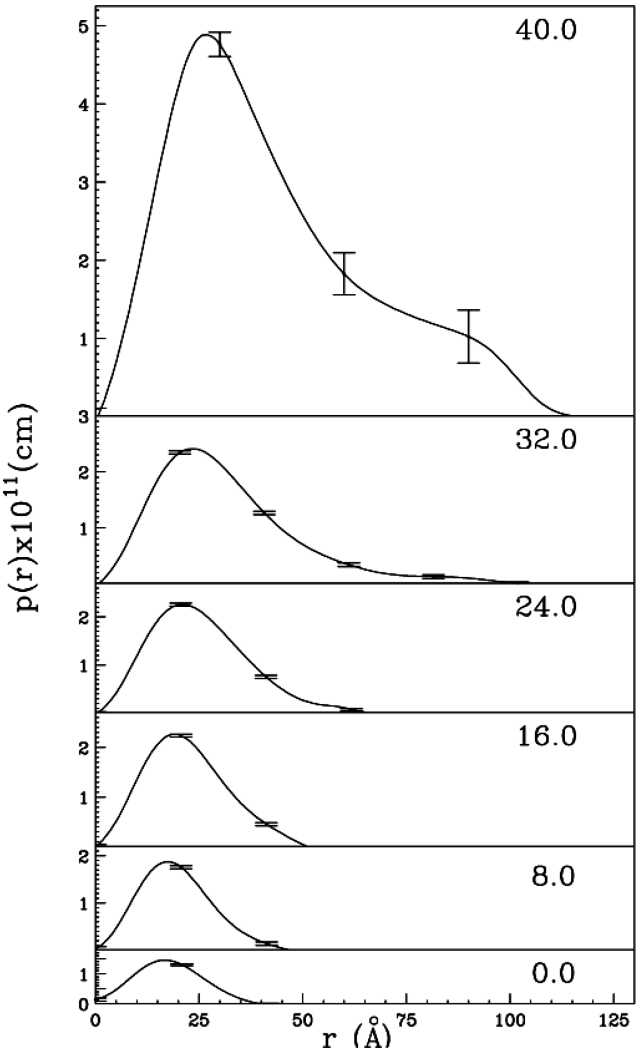

Figure 3. Experimental $p(r)$ functions of NaGC + NaGDC (40 mM) at NaCl 0.6 M. Only the NaGDC concentrations (mM) are reported. For clarity only a few error bars are shown.

could arise because of a significant growth of the aggregates with respect to the reference NaGDC 40 mM sample. The decreasing trend of the particle sizes, testified by the progressive decrease of the R_g and D_M values, with the NaGDC concentration decreasing (Figure 4 and Table 1), allows us to rule out this hypothesis.

DLS of Two-Component (NaGC and NaGDC) Samples. The observed apparent mean hydrodynamic radius values together with R_g is reported vs NaGDC concentration in Figure 4. As mentioned in the discussion of the SAXS data, the R_h data reflect a change in both size and shape of the micelles. To compare SAXS and DLS data a hydrodynamic radius R_h^{OG} was estimated with the method of Ortega and Garcia de la Torre[50] on the basis of the SAXS parameters of Table 1. In particular, cylindrical micelles of diameter $= 2\sqrt{2}R_c$and height h were assumed. The results show that the consistency between R_h and R_h^{OG} decreases by increasing the NaGC concentration (Table 1). A reasonable agreement was observed for NaGDC concentration $\geq$24 mM where an elongated shape of the micelles could still be expected. The inconsistency shown by the other samples confirms that a drastic variation of the micelle structure toward the NaGC pure micelle shape takes place by increasing the NaGC concentration.

ESIMS Spectra of Two-Component (NaGC and NaGDC) Samples in Positive-Ion Detection Mode. This section reports results obtained submitting to ESIMS five solutions containing different molar ratios of NaGDC (D) and NaGC (G) bile salts. The solutions were named as follows: (1) 0D (0% D, that is 100% G); (2) 25D (25% D + 75% G); (3) 50D (50% D + 50% G); (4) 75D (75% D + 25% G); and (5) 100D (100% D), where the percentages refer to the molar composition. The starting total analyte concentration was 10^{-3} M (diluted solutions) and 10^{-2} M (concentrated solutions).

Abundant gas phase bile salts cluster ions were observed for the three mixed solutions (25D, 50D, and 75D) under HNS conditions, and a general trend can be noted concerning the variety and abundances of the observed positively charged cluster ions.[51,52] In Figure 5 a typical spectrum, relative to the equimolar solution of D and G bile salts (50D, 10^{-3} M) is reported. It is a representative example of the mass spectra collected during this investigation and will be used to illustrate the spectral analysis. The main series of peaks, extending over the entire mass range investigated, is denoted as M_n^{b+} and can be attributed to singly charged aggregates of mixed bile salts containing up to 10 bile salt units. M indicates a bile salt, that can be either D or G, n is the number of bile salt molecules defining the multimer family ($n = 1-10$), and b is the number of additional sodium ions that determine the aggregate charge state. The greater complexity of this spectrum, if compared to those of one component solutions,[34] is due to the different possible combinations of the two bile salts, D and G, within each multimer. Each family of M_n^+ aggregates is, in fact, composed by $n + 1$ peaks, and peaks within each family correspond to bile salt aggregates with the same total number of n, but having a different composition of D and G units. As an example, the trimer family M_3^+ contains 4 peaks corresponding to the formula $[D_xG_y]Na^+$ (x, $y = 0-3$ and $x + y = 3$), each having the following specific composition in bile salts: D_3, D_2G, DG_2, and G_3. When using this symbology the charge state and thus the sodium units are omitted for the sake of simplicity. An example relative to the tetramers is reported in the inset of Figure 5.

Due to the decrease in cluster abundance with increasing mass, the highest m/z peaks which could be confidently assigned were those relative to the hexamer family M_6^+. In fact, the noise in the high mass range is likely caused by unresolved cluster ions coming from a large range of x and y possible combinations, and also to the contribution of multiply charged ions, possibly present at higher mass.

Consistent with this, the examination of the spectra reveals a second series of cluster ions as evidenced by ionic signals located halfway between singly charged ion clusters and corresponding to doubly charged species. The lowest mass peak of this series, despite its very low abundance, is found between the $n = 3$ and 4 peaks, and is assigned to the M_7^{2+} cluster. The next cluster in this series is M_8^{2+} and has the same m/z ratio as M_4^+. Multiply charged clusters may be hidden in mass spectra because of an overlap in m/z with singly charged ions. A closer inspection of peaks distribution showed, indeed, a very small contribution of M_8^{2+} to the M_4^+ tetramer. A third series, much less intense than the previous one, corresponding to the triply charged ions, appears only when $x + y = 13$, that is M_{13}^{3+}.

Thus, peaks belonging to singly and multiply charged species can all be identified by the formula $[D_xG_y]Na_b^{b+}$, where $x + y = n$ identifies the cluster family M_n, and b is the number of sodium ions that determines the charge state of the aggregates.

TABLE 1: Most Relevant Parameters of the SAXS Spectra Recorded at 25 °C and NaCl Concentration 0.6 M[a]

NaGDC	R_g	R_c	D_M	h	h^*	R_h	R_h^{OG}
40	33.0	12.8	115	105	108	36.0	33
32	25.7	12.7	95	77	69	27.1	28
24	19.7	11.7	65	55	53	21.2	23
16	16.7	10.5	50	45	46	17.7	20
8	14.8	9.4	45	40	40	15.7	18
0	13.5	8.7	38	36	36	13.6	16

[a] All the values are in Å except those of the first column which are NaGDC concentrations in mM. Esd's are within 2% (R_g, R_c), 5% (R_h, h^*), and 10% (D_M).

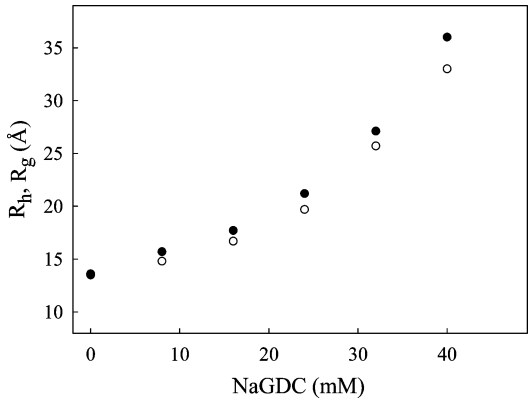

Figure 4. Experimental R_h (black circles) and R_g (open circles) as a function of NaGDC concentration. NaGC concentration is given by 40 − NaGDC concentration.

In the following, our discussion will be focused only on singly charged multimer ions M_n^+.

The relative intensities of multimer ions, M_n^+, in all systems investigated are shown in Figure 6, part A (diluted solutions) and part B (concentrated solutions).

In the case of mixed solutions, M_n^+ intensities are considered as the sum of all the peaks composing each family. Relative intensities are not much affected by the starting concentration, nor is the onset of production of multiply charged cluster ions. In fact, with both 10^{-3} and 10^{-2} M solutions the main difference between mixed and pure bile salt systems is that in the former the most intense multimer family is always the trimer M_3^+, followed by comparable amounts of M_1^+ and M_2^+ species, the dimer family slightly exceeding the monomer only in the concentrated 25D solution. Differently, dimer is the most abundant ion in the 0D solution, while trimer is the most intense in 100D. Multimers with $n = 4$ to 6 are slightly more abundant in solutions with increasing D percentage pointing to a higher aggregation ability of glycodeoxycholate compared to glycocholate.

In order to analyze the internal distribution, that is, the specific composition of each multimer family, we will begin by examining the three mixtures at the same 10^{-3} M concentration (diluted solutions), highlighting the effect of the relative ratio of the two bile salts. Then, we will take into account the effect of total bile salts concentration on the internal distribution by examining the concentrated solutions (10^{-2} M). Specific composition and relative intensities of peaks within each multimer family, in all systems investigated, are reported in Table 2. In each system the third column reports the relative frequency peaks distributions that would be expected assuming a binomial distribution of D and G units into the aggregates. These values are used in the following discussion as a comparison with the experimental relative intensities of peaks in each multimer family. A graphical representation of all values relevant to the M_4^+ and M_5^+ families can be found in Figure 7. Referring to all the three mixed diluted solutions 25D, 50D, and 75D, we immediately note that the relative intensities among clusters within each family deviate from the expected distribution, with the exception of M_3^+.

M_1^+ and M_2^+ deviate since G-containing cluster are more abundant; G is always slightly higher with respect to D in monomers, and dimers prefer to form G_2. G aggregating ability drives monomers and dimers behavior in these two families. Starting with tetramers an opposite trend is observed. The M_4^+−M_6^+ families in the equimolar system (50D) display a skewed distribution toward clusters containing more D units, suggesting a preferential aggregation of clusters that are enriched with D bile salts, and correspondingly depleted in G. This behavior is enhanced with increasing n, the number of bile salt species. As an example in the M_5^+ family D_5 is twice G_5 (10.6 vs 4.7) and in M_6^+ family G_6 is even absent.

A more dramatic example of this behavior is given below. When we compare multimers of 25D and 75D systems, if D and G were combined randomly, inverted distributions of peaks would be expected for each family (as an example the intensities of tetramers have the same values in 25D and 75D but in a reverse order). Indeed, we did not observe such a pattern; both systems reveal a displacement of clusters that favors incorporation of D units. It is particularly evident in the 25D system where the distribution clearly moves toward D-containing clusters, compared to the probabilistic distribution. Taking as an example the tetramer family, in 25D D_4 is by far higher than its expected value (5.4 vs 0.40), but in 75D G_4 is absent, or D_3G in 25D is more intense than DG_3 in 75D, whereas in both examples, according to their expected values, they should be identical.

The higher aggregation ability of D is even more pronounced in the results on the concentrated solution (10^{-2} M). The bile salt concentration affects cluster distribution, within each multimer family, in the same way along the three systems but with a different strength. At lower D percentages, we observe a greater shift toward cluster containing more D units. In other words, this effect is almost negligible in 75D, with multimers showing a practically identical cluster distribution in either diluted or concentrated solutions. The 25D system suffers the maximum concentration effect, showing aggregate ions with compositions that favor incorporation of D bile salts. The result, in this system and also in 50D, is a population more representative of species enriched with D units. As an example, considering the 50D system, D_5 increases from being twice G_5 in 10^{-3} M to 10 times G_5 in the concentrated solution.

Finally, it is interesting to note that an effect on cluster distribution almost similar to that obtained with increasing concentration can be obtained by agitating 10^{-3} M solutions; in this case cluster distribution resembles that obtained in 10^{-2} M.

When the voltage difference is decreased (LNS conditions), the total ion current is reduced, so that concentrated solutions, 10^{-2} M, and flow rates of 20 μL/min are needed, preventing any comparison with diluted solutions. Ion signals appear predominantly in the low-mass region, up to 2000 Da, with a

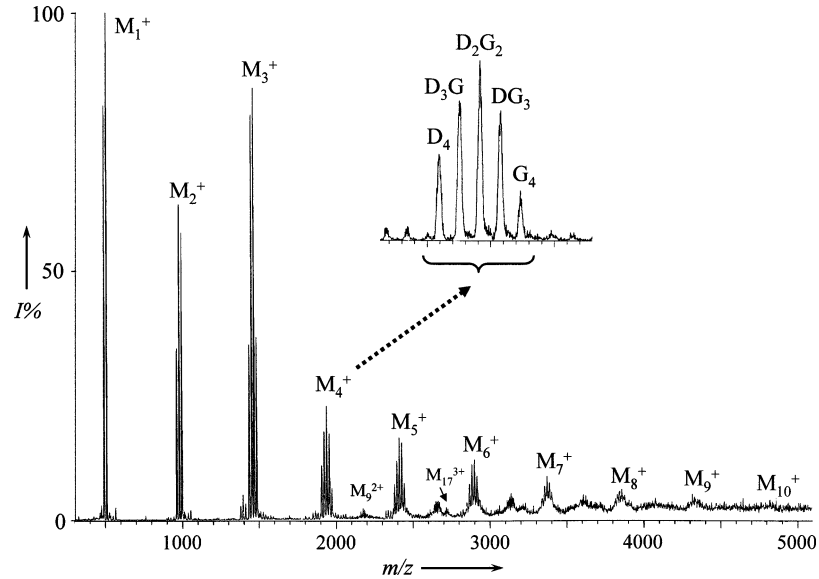

Figure 5. Mass spectrum of 50D dilute aqueous solution (HNS conditions). The inset shows the detailed composition of tetramers.

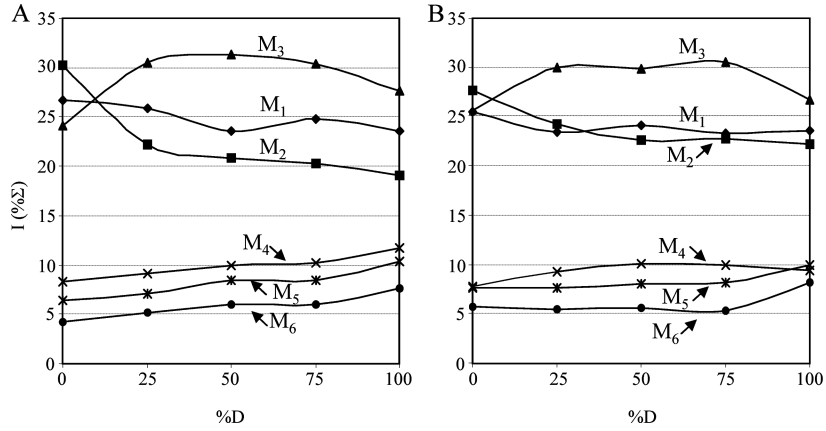

Figure 6. Intensity plot of the $M_1^+-M_6^+$ species as a function of glycodeoxycholate concentration in diluted (A) and concentrated (B) solutions.

displacement to lower mass of the multiply charged ionic population. In fact, charge state analysis reveals a contribution of M_4^{2+} to the dimer M_2^+, the monomer M_1^+ being the only singly charged ions present in the spectra. The first triply charged ions are M_7^{3+}.

Concerning peak distributions, only the analysis on the M_2^+ family is possible, showing a common feature of the three systems. Clusters containing more G molecules, that is, G_2, are even less intense than D-containing clusters, with respect to the HNS conditions, suggesting a preferential aggregation of D-containing species. Unfortunately, we cannot assess whether this behavior can be extended to all other M_n^+ families. Peaks relative to these cluster ions appear broad and unresolved; these features arise from the overlap of the array of cluster sizes and charge states.

An estimation of the composition in NaGDC/NaGC mixture solutions was attempted in already published EMF measurements[37] by following previously described procedures.[53,54] The proposed typical anionic compositions of the mixed aggregates are D_3G_2, D_9G_4, $D_{18}G_8$, $D_{36}G_8$, and $D_{54}G_8$, showing that even (2, 4, and 8) or multiple of three (3, 9, 18, 36, and 54) anion numbers are preferred by glycocholate or glychodeoxycholate, respectively. Although related to the same bile salt mixture, it is important to remark that the EMF and ESIMS compositions cannot be strictly compared. The main reasons are that (i) to apply the constant ionic medium method tetramethylammonium chloride (TMACl) is present (in the concentration range 0.10−0.75 M) in the EMF samples in order to replace activity with concentrations in the calculations,[55] whereas ESIMS samples are prepared in pure water; (ii) the actual concentration and pH of the ESIMS measurements are unknown,[34,51] whereas they are well-defined in the samples analyzed by EMF; (iii) the EMF data interpretation was performed by assuming the least number of species; and (iv) the ESIMS species are positively charged at variance with the aggregates studied by SAXS, DLS, and EMF.

Moreover, the EMF results, although able to provide reliable overall aggregation numbers of the species which are subject to several equilibrium constrains, are not rigidly conditioned by the aggregate compositions. This means that a possible interchange between the bile salt anions within an aggregate cannot be discarded, namely that, assuming an uncertainty x, an anion aggregate D_mG_n could be formed, for instance, by $n + x$ G and $m - x$ D or by $n - x$ G and $m + x$ D. A very interesting point of the EMF measurements is that in all the aggregates the Na^+ numbers are greater than 50% of the anion numbers, thus suggesting a greater Na^+ fractional binding with respect to TMA^+.[56] In this connection, it must be remembered that a bigger size of the aggregates is observed for NaGDC + NaCl samples as compared with NaGDC + TMACl or with

TABLE 2: Internal Composition of M_n^+ Families[a]

	system									
		25D			50D			75D		
species	0D	dilute	conc	F_{exp}	dilute	conc	F_{exp}	dilute	conc	F_{exp}	100D
monomers											
D	–	22.0	32.5	25.0	42.6	50.8	50.0	65.0	67.9	75.0	100
G	100	78.0	67.5	75.0	57.4	49.2	50.0	35.0	32.1	25.0	–
dimers											
D_2	–	8.1	15.6	6.2	22.6	31.8	25.0	47.3	51.1	56.3	100
DG	–	29.0	36.2	37.5	38.9	40.0	50.0	37.8	35.2	37.5	–
G_2	100	62.9	48.2	56.3	38.5	28.1	25.0	14.9	13.7	6.2	–
trimers											
D_3	–	4.0	8.7	1.6	14.4	20.7	12.5	36.7	38.9	42.2	100
D_2G	–	17.8	26.6	14.0	33.6	36.7	37.5	41.4	40.5	42.2	–
DG_2	–	39.1	39.2	42.2	36.5	31.9	37.5	18.5	17.7	14.0	–
G_3	100	39.1	25.5	42.2	15.4	10.7	12.5	3.4	2.8	1.6	–
tetramers											
D_4	–	5.4	7.5	0.40	13.1	19.7	6.2	38.2	39.2	31.6	100
D_3G	–	9.8	17.3	4.7	24.2	28.3	25.0	35.3	35.9	42.2	–
D_2G_2	–	21.7	28.0	21.1	31.3	29.3	37.6	19.6	19.2	21.1	–
DG_3	–	34.8	30.9	42.2	23.2	17.8	25.0	6.9	5.8	4.7	–
G_4	100	28.3	16.2	31.6	8.2	4.8	6.2	–	–	0.40	–
pentamers											
D_5	–	–	5.4	0.1	10.6	14.4	3.1	32.6	33.8	23.7	100
D_4G	–	7.1	11.0	1.5	20.0	23.0	15.6	33.7	36.2	39.6	–
D_3G_2	–	14.3	20.6	8.8	27.1	29.3	31.3	21.7	22.1	26.3	–
D_2G_3	–	25.7	29.7	26.3	24.7	22.8	31.3	8.4	8.0	8.8	–
DG_4	–	32.8	24.7	39.6	12.9	9.0	15.6	3.6	–	1.5	–
G_5	100	20.1	8.6	23.7	4.7	1.6	3.1	–	–	0.1	–
hexamers											
D_6	–	–	2.9	0.024	8.3	9.7	1.6	26.2	24.8	17.8	100
D_5G	–	5.7	7.2	0.44	15.0	17.3	9.4	34.4	34.9	35.6	–
D_4G_2	–	9.4	13.2	3.34	21.7	26.5	23.4	26.2	28.9	29.6	–
D_3G_3	–	17.0	24.2	13.2	26.7	26.8	31.2	13.2	11.4	13.2	–
D_2G_4	–	26.4	29.9	29.6	20.0	16.6	23.4	–	–	3.34	–
DG_5	–	28.3	16.7	35.6	8.3	5.1	9.4	–	–	0.44	–
G_6	100	13.2	5.1	17.8	–	–	1.6	–	–	0.024	–

[a] Frequencies expected on a probabilistic basis (F_{exp}) are also shown. The uncertainties of the peak intensities are within 15%.

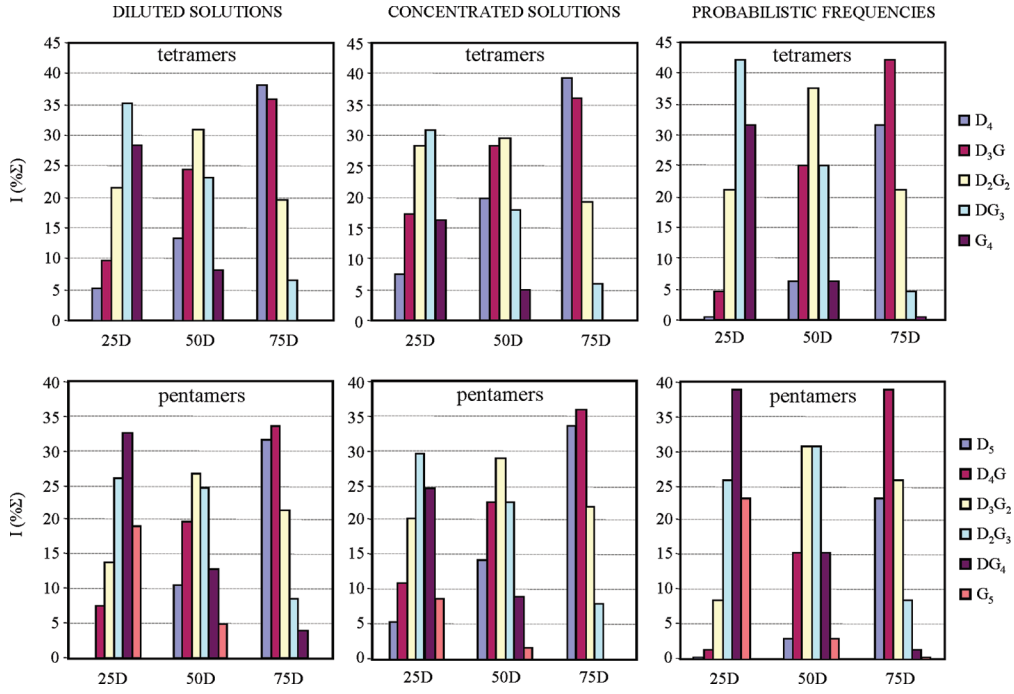

Figure 7. Intensity plot of the peaks distribution in the M_4^+ and M_5^+ species in diluted and concentrated mixtures. For comparison purposes the probabilistic frequencies are also shown.

tetramethylammonium glycodeoxycholate (TMAGDC) + TMACl solutions at a fixed concentration and ionic strength.[57] Moreover, X-ray, circular dichroism, DLS, electrolytic conductance, and dielectric results converge in outlining similar structural models

(7/1 helices) for the NaGDC and TMAGDC anion aggregates, despite their different size. Both cations (Na^+ and TMA^+) chiefly interact by means of polar forces with the anion aggregates, but Na^+ is more firmly bound to the anion aggregates than TMA^+, the binding of which probably interrupts the aggregate growth.[57] According to this assertion, the following R_h values trends of the micellar aggregates NaGDC > RbGDC > TMAGDC;[57,58] NaTDC > RbTDC > TMATDC;[29] LiDC > NaDC > KDC > RbDC were observed and explained in terms of a decreasing cation affinity for anion aggregates by decreasing the cation charge density.[29] For the last series (deoxycholate salts) the X-ray analysis of their fibers supported the affinity order.[59]

Conclusions

The SAXS and QELS experiments on NaGC/NaGDC mixtures suggest that micelles are formed whose size decrease by increasing the NaGC fraction. For the pure NaGDC samples cylindrical aggregates are observed. The lowering of the size induced by NaGC is accompanied by a progressive change of the aggregate morphology toward the small globular-like shape of the pure NaGC aggregates. ESIMS measurements suggest that, in the pure samples, the glycocholate and glycodeoxycholate anions preferably aggregate in dimers and trimers, respectively. In the mixtures, the ESIMS experiments permit to establish the oligomer composition, showing that mixed aggregates are formed where the anion ratio is not statistical, namely not governed only by NaGDC and NaGC concentrations. The process driving force depends also on the free energy gain associated with the glycodeoxycholate and glycocholate transfer from the bulk electrolyte aqueous solution to the anion aggregate. Reasonably, the glycodeoxycholate one is less than that of glycocholate (one hydroxyl group more). This conclusion justify the greater glycodeoxycholate aggregating ability.

Acknowledgment. We thank MIUR for the financial support (PRIN project 2006 039789-001) and CASPUR for technical support. The authors acknowledge the ESRF for the financial support (proposal SC1233) and the Dutch-Belgian Beamline (DUBBLE) research group at the ESRF, France, for their help and support.

References and Notes

(1) Hofmann, A. F.; Small, D. M. *Annu. Rev. Med.* **1967**, *18*, 333.
(2) Small, D. M. In *The Bile Acids*; Nair, P. P., Kritchevsky, D., Eds.; Plenum Press: New York, 1971; Vol. 1; pp 249−356.
(3) Carey, M. C. In *The Liver: Biology and Pathobiology*; Arias, I. M., Popper, H., Schacter, D., Shafritz, D., Eds.; Raven Press: New York, 1982; pp 429−465.
(4) Carey, M. C. In *Sterols and Bile Acids*; Danielsson, H., Sjøvall, J., Eds.; Elsevier/North-Holland Biomedical Press: Amsterdam, 1985; pp 345−403.
(5) Funasaki, N.; Fukuba, M.; Kitagawa, T.; Nomura, M.; Ishikawa, S.; Hirota, S.; Neya, S. *J. Phys. Chem. B* **2004**, *108*, 438.
(6) Jover, A.; Meijide, F.; Rodríguez Núñez, E.; Vázquez Tato, J.; Mosquera, M.; Rodríguez Prieto, F. *Langmuir* **1996**, *12*, 1789.
(7) Li, Y.; Holzwarth, J. F.; Bohne, C. *Langmuir* **2000**, *16*, 2038.
(8) Hebling, C. M.; Thompson, L. E.; Eckenroad, K. W.; Manley, G. A.; Fry, R. A.; Mueller, K. T.; Strein, T. G.; Rovnyak, D. *Langmuir* **2008**, *24*, 13866.
(9) Matsuoka, K.; Maeda, M.; Moroi, Y. *Colloids Surf. B: Biointerfaces* **2003**, *32*, 87.
(10) Marques, E. F.; Edlund, H.; La Mesa, C.; Khan, A. *Langmuir* **2000**, *16*, 5178.
(11) Jean, B.; Oss-Ronen, L.; Terech, P.; Talmon, Y. *Adv. Mater.* **2005**, *17*, 728.
(12) Terech, P.; de Geyer, A.; Struth, B.; Talmon, Y. *Adv. Mater.* **2002**, *14*, 495.
(13) Youssry, M.; Coppola, L.; Furia, E.; Oliviero, C.; Nicotera, I. *Phys. Chem. Chem. Phys.* **2008**, *10*, 6880.
(14) Long, M. A.; Kaler, E. W.; Lee, S. P.; Wignall, G. D. *J. Phys. Chem.* **1994**, *98*, 4402.
(15) Pedersen, J. S.; Egelhaaf, S. U.; Schurtenberger, P. *J. Phys. Chem.* **1995**, *99*, 1299.
(16) Arleth, L.; Bauer, R.; Øgendal, L. H.; Egelhaaf, S. U.; Schurtenberger, P.; Pedersen, J. S. *Langmuir* **2003**, *19*, 4096.
(17) Luk, A. S.; Kaler, E. W.; Lee, S. P. *Biochemistry* **1997**, *36*, 5633.
(18) Youssry, M.; Coppola, L.; Marques, E. F.; Nicotera, I. *J. Colloid Interface Sci.* **2008**, *324*, 192.
(19) Marques, E. F.; Regev, O.; Edlund, H.; Khan, A. *Langmuir* **2000**, *16*, 8255.
(20) Terech, P.; Sangeetha, N. M.; Maitra, U. *J. Phys. Chem. B* **2006**, *110*, 15224.
(21) Terech, P.; Maitra, U. *J. Phys. Chem. B* **2008**, *112*, 13483.
(22) Vijayalakshmi, N.; Maitra, U. *Macromolecules* **2006**, *39*, 7931.
(23) Soto Tellini, V. H.; Jover, A.; Meijide, F.; Vázquez Tato, J.; Galantini, L.; Pavel, N. V. *Adv. Mater.* **2007**, *19*, 1752.
(24) Alvarez Alcalde, M.; Jover, A.; Meijide, F.; Galantini, L.; Pavel, N. V.; Antelo, A.; Vázquez Tato, J. *Langmuir* **2008**, *24*, 6060.
(25) Galantini, L.; Giglio, E.; Pavel, N. V. *J. Phys. Chem. B* **2005**, *109*, 9849.
(26) Funasaki, N.; Fukuba, M.; Kitagawa, T.; Nomura, M.; Ishikawa, S.; Hirota, S.; Neya, S. *J. Phys. Chem. B* **2005**, *109*, 9851.
(27) D'Alagni, M.; Galantini, L.; Gavuzzo, E.; Giglio, E.; Scaramuzza, L. *J. Chem. Soc., Faraday Trans.* **1994**, *90*, 1523.
(28) Bottari, E.; D'Archivio, A. A.; Festa, M. R.; Galantini, L.; Giglio, E. *Langmuir* **1999**, *15*, 2996.
(29) Briganti, G.; D'Archivio, A. A.; Galantini, L.; Giglio, E. *Langmuir* **1996**, *12*, 1180.
(30) Galantini, L.; Giglio, E.; La Mesa, C.; Pavel, N. V.; Punzo, F. *Langmuir* **2002**, *18*, 2812.
(31) Cole, R. B. *J. Mass Spectrom.* **2000**, *35*, 763.
(32) Kebarle, P. *J. Mass Spectrom.* **2000**, *35*, 804.
(33) *Electrospray Ionization Mass Spectrometry*; Cole, R. B., Ed.; Wiley: New York, 1997.
(34) Cacace, F.; de Petris, G.; Giglio, E.; Punzo, F.; Troiani, A. *Chem.−Eur. J.* **2002**, *8*, 1925.
(35) Galantini, L.; Giglio, E.; Pavel, N. V.; Punzo, F. *Langmuir* **2003**, *19*, 1319.
(36) Galantini, L.; Giglio, E.; Pavel, N. V.; Punzo, F. *Colloids Surf. A: Physicochem. Eng. Aspects* **2004**, *248*, 79.
(37) Bottari, E.; Festa, M. R. *Ann. Chim. (Rome)* **2005**, *95*, 791.
(38) Bras, W. *J. Makromol. Sci., Phys.* **1998**, *B 37*, 557.
(39) Blanton, T. N.; Huang, T. C.; Toraya, H.; Hubbard, C. R.; Robie, S. B.; Louer, D.; Goebel, H. E.; Will, G.; Raftery, T. *Powder Diffr.* **1995**, *10*, 91.
(40) Glatter, O. In *Small Angle X-ray Scattering*; Glatter, O., Kratky, O., Eds.; Academic Press: London, 1982.
(41) Koppel, D. E. *J. Chem. Phys.* **1972**, *57*, 4814.
(42) Siegert, A. J. F. "On the fluctuations in signals returned by many independent, moving scatterers"; Report No 465, MIT (Mass. Inst. Technol.) Radiation Lab., 1943; pp 1−14.
(43) Janich, M.; Lange, J.; Graener, H. *J. Phys. Chem. B* **1998**, *102*, 5957.
(44) Galantini, L.; Giglio, E.; Leonelli, A.; Pavel, N. V. *J. Phys. Chem. B* **2004**, *108*, 3078.
(45) Cozzolino, S.; Galantini, L.; Giglio, E.; Hoffmann, S.; Leggio, C.; Pavel, N. V. *J. Phys. Chem. B* **2006**, *110*, 12351.
(46) Campanelli, A. R.; Candeloro De Sanctis, S.; Galantini, L.; Giglio, E. *J. Inclusion Phenom. Mol. Recognit. Chem.* **1991**, *10*, 367.
(47) Bonincontro, A.; D'Archivio, A. A.; Galantini, L.; Giglio, E.; Punzo, F. *Langmuir* **2000**, *16*, 10436.
(48) Durchschlag, H.; Zipper, P. *J. Com. Esp. Deterg.* **1995**, *26*, 275.
(49) Leggio, C.; Galantini, L.; Zaccarelli, E.; Pavel, N. V. *J. Phys. Chem. B* **2005**, *109*, 23857.
(50) Ortega, A.; Garcia de la Torre, J. *J. Chem. Phys.* **2003**, *119*, 9914.
(51) Siuzdak, G.; Bothner, B. *Angew. Chem.* **1995**, *34*, 2053.
(52) Rodriguez, M. A.; Yost, R. A. *Rapid Commun. Mass Spectrom.* **2000**, *14*, 1398.
(53) Bottari, E.; Festa, M. R. *Langmuir* **1996**, *12*, 1777.
(54) Bottari, E.; Festa, M. R.; Franco, M. *Langmuir* **2002**, *18*, 2337.
(55) Biedermann, G.; Sillèn, L. G. *Ark. Kemi* **1953**, *5*, 425.
(56) Bottari, E.; Festa, M. R. *Monatsh. Chem.* **1993**, *124*, 1119.
(57) D'Archivio, A. A.; Galantini, L.; Gavuzzo, E.; Giglio, E.; Punzo, F. *Langmuir* **2001**, *17*, 4096.
(58) Campanelli, A. R.; Candeloro De Sanctis, S.; Chiessi, E.; D'Alagni, M.; Giglio, E.; Scaramuzza, L. *J. Phys. Chem.* **1989**, *93*, 1536.
(59) Bonincontro, A.; D'Archivio, A. A.; Galantini, L.; Giglio, E.; Punzo, F. *J. Phys. Chem. B* **1999**, *103*, 4986.

JP9010586